Low Noise Magnetic Fields in Ultracold Experiment

by

Eber Nolasco-Martinez

Submitted to the Department of Physics
in partial fulfillment of the requirements for the degree of

Bachelor of Science in Physics

at the

MASSACHUSETTS INSTITUTE OF TECHNOLOGY

May 2020

Author .....
Department of Physics
May 11, 2020

Certified by .....
Wolfgang Ketterle
Professor of Physics
Thesis Supervisor

Accepted by .....
Nergis Mavalvala
Associate Department Head, Department of Physics

Low Noise Magnetic Fields in Ultracold Experiment

by

Eber Nolasco-Martinez

Submitted to the Department of Physics
on May 11, 2020, in partial fulfillment of the
requirements for the degree of
Bachelor of Science in Physics

Abstract

Ultracold atomic and molecular experiments rely on low noise ambient magnetic fields for precision spectroscopy and studying Feshbach resonances with narrow linewidths, which can be on the order of 1 μT. The ambient field is impacted by both the Earth's magnetic field and technical noise from surrounding electrical equipment, which can vary through the day. We built an apparatus using an Arduino microprocessor to record the ambient fields with magnetometers located outside the vacuum chamber containing the atoms and output transformed waveforms at 30 Hz intervals to be feedforwarded to the coils and cancel both the average field and fluctuations. We achieved an RMS of 37 nT along one axis in the magnetic fields in our test setup using this apparatus, reducing the 60 Hz component by 30 dB and the 180 Hz component by 20 dB.

Thesis Supervisor: Wolfgang Ketterle
Title: Professor of Physics

Acknowledgments

I would first like to thank Dr. Wolfgang Ketterle and Dr. Alan Jamison for providing both the opportunity to work in this lab and for their guidance in both my physics career and in producing this thesis. I would then like to thank the members of the BEC3 and Dypole lab for explaining the physics and electronics behind their projects, advice on applying to graduate school, general mentorship, and guidance in advancing this project. These include Hyungmok Son, Julie Park, Pierre Barral, Will Lunden, Li Du, and Michael Cantara, who helped me significantly in organizing and writing this thesis. I would also like to thank fellow undergraduate Rokas Veitas, who also worked on this project with me and wrote a significant portion of the code used. Lastly, I would like to thank my parents, who worked hard to care for me and my siblings in the hope that we grow strong, intelligent, and healthy, as well as the friends that I've made here at MIT, The Tech, and at Random Hall, who made my time here worthwhile, whom I will miss as I graduate and advance onto the next stage of my career, and whom I hope to see again sometime soon.

Contents

Chapter 1

Introduction

Ultracold atoms and molecules experiments are an ever-growing avenue of research. Originating from research in the 1990's to produce Bose-Einstein condensates under Wolfgang Ketterle [1], Eric Cornell, and Carl Wieman [2], ultracold atomic experiments has advanced today to a large field that promises to explore a variety of topics at micro and nanoKelvin temperatures, including dipolar interactions, quantum computation, quantum metrology, and many-body condensed matter physics [3]. Ultracold molecules are especially of interest because they are capable of holding permanent electric and magnetic dipole moments and thus the interactions between particles can be controlled, which can be useful for studying quantum computation and molecular dynamics [4].

Ultracold systems, in general, provide a simple system to analyze quantum mechanics under model Hamiltonians. It is, however, not as simple to produce the conditions necessary for a batch of ultracold particles. Any such apparatus requires a large assortment of optics, electronics, lasers, and magnetic coils to capture and manipulate the particles. A lot of work is needed in creating feedback systems to ensuring low noise in the laser's intensity and frequency, in the magnetic fields, and in the imaging apparatus to minimize heating and maximize particle count. In order to do so, however, requires a strong knowledge of the interactions involved between the atoms, photons, and magnetic fields.This becomes even more difficult to understand when one tries to go beyond alkali atoms to systems that can contain even more

complex electronic structures and possible reaction pathways [5].

In order to produce quantum degenerate systems of particles, a wide variety of techniques utilizing lasers and magnetic fields are employed. Such techniques include varying the magnetic field to change the resonant frequency in a Zeeman slower, creating a quadrupole field to catch atoms in a magneto-optical trap and in a magnetic well, and using Feshbach resonance to create a spectroscopy of atomic energy levels and produce ultracold molecules.

To perform these techniques, multiple coils and lasers have to be brought in, increasing the necessity of accounting for noise in the magnetic field. This is especially true for experiments that require sensitive measurements. As such, it is becoming increasingly important to understand and treat the impact of environmental magnetic field noise on the experiments as we try to achieve more accurate measurements of the interactions studied. Therefore, this thesis's goal is to describe the effort to reduce these environmental fields using active feedforward and explain how it is expected to improve ultracold atomic experiments.

1.1 Organization

This thesis will serve to explain the physics behind ultracold molecular experiments and motivate the necessity and method for canceling environmental magnetic fields fields.

Chapter 2 will first discuss the physics and motivation for studying degenerate atomic systems.

Chapter 3 describes the procedures and techniques used for trapping and producing ultracold atoms and molecules.

Chapter 4 discusses Feshbach resonance and chapter 5 introduces the concept of STIRAP, both necessary ingredients for producing ultracold molecules and controlling the dynamics of ultracold atoms.

Chapter 6 will go into a description of the active magnetic field stabilization procedure and apparatus.

Chapter 7 will summarize the results in performance and describe what future progress can be made.

Chapter 2

Quantum Degeneracy of Bosons and Fermions

Before we begin discussing further about creating ultracold molecules, let us talk about the ideas behind quantum degeneracy at low temperature. This discussion is based on the lecture notes and slides provided by Dr Xiao-Gang Wen in MIT's 8.08 Class in the Spring of 2019 [6].

When considering the distribution of particle energies at a given temperature, we usually use the partition function where each energy state is given a probability proportional to the Boltzmann factor e^{-E_i/k_BT}. Thus for any classical gas, we expect each particle to be independent and the probability of any given energy state to be given by the Boltzmann factor, even at very low temperatures. However, this turns out to be quite false when dealing at the quantum level. The main reason for this is that particles are indistinguishable, which impacts the particle statistics at low temperature. For bosons, we find that the particles tend to group together, so that when T is low enough, nearly all the particles go to the ground state. In contrast, fermions refuse to have multiple particles in an identical state so they begin to fill up each individual energy state from the bottom, as shown in 2-1.

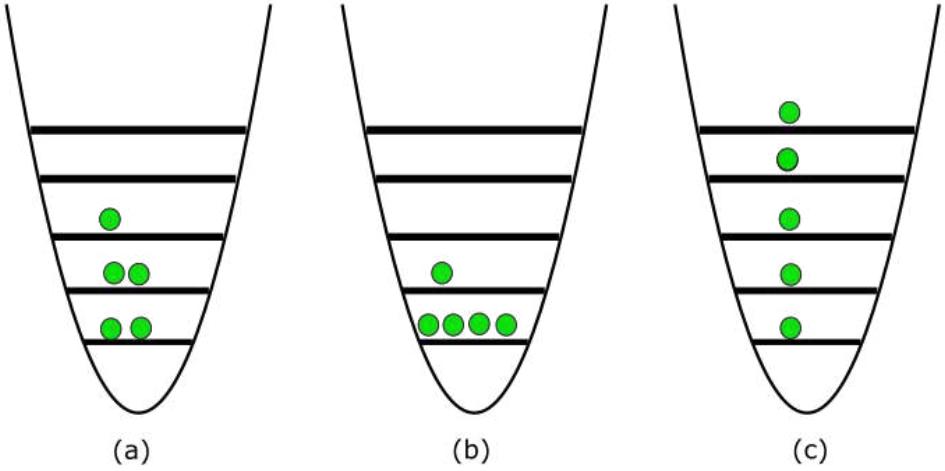

Figure 2-1: The statistics of the particles create different distributions among the energy levels at low temperature, as seen above with (a) distinguishable particles, (b) bosons, and (c) fermions.

2.1 Bose-Einstein Condensates

Let us develop this intuition by first consider a collection of N atoms within a box of size $V = L^3$. In this case, each atom is only allowed to have wavevectors $k = \frac{2\pi n}{L}$ for integer n and energies $E = \hbar ck$.

For classical, distinguishable particles, we can assign for each particle their independent state, giving states $|\Psi\rangle = |\psi_1\rangle|\psi_2\rangle...|\psi_n\rangle$. However, we find that for many quantum particles, when their properties are identical, two particles cannot be distinguished, impacting their statistics. As such, the wavefunction of two particles are equivalent when switched, besides an overall phase factor, and that sign can depend on the spin of the particle. For particles of integer spins, or bosons, we find that switching particles give a phase factor of 1. For half-integer spins, or fermions, the wavefunction gets a phase factor of -1.

When particles are bosons, we find that, in order for the overall wavefunction to

be valid, we require the particle to be symmetric over exchanges between all particles, so we instead are required to be in a superposition of all possible exchanges, with

$$|\Psi\rangle = K(|\psi_1\rangle|\psi_2\rangle...|\psi_n\rangle + |\psi_2\rangle|\psi_1\rangle...|\psi_n\rangle + ... \tag{2.1}$$

where K is a normalization factor and the terms include all permutations of the states of each boson.

We find that another valid and more useful representation for bosons is second quantization, where we instead consider the possible energy levels of a single particle and simply count the number of particles in each level to distinguish a state. Thus if we have five bosons in the ground state and three bosons in the excited state, we simply denote the total state as $|\Psi\rangle = |n_0 = 5, n_1 = 3\rangle$.

Each boson provides an energy corresponding to their state, so $E = \sum n_k \epsilon_k$. Each individual state for a boson then acts likes an independent simple harmonic oscillator or SHO whose excitation level depends on the number of bosons in each state. The partition function for an SHO is then

$$Z_k = \sum e^{-\frac{n_k \hbar \omega_k}{k_B T}} = \frac{1}{1 - e^{-\frac{\hbar \omega_k}{k_B T}}}. \tag{2.2}$$

For a photon, the product of all such SHO is sufficient to provide the full partition, but for massive bosons with fixed quantum number, we use the grand canonical ensemble picture to fix the number of bosons by defining μ, the chemical potential, as the energy needed to add an additional boson. Then

$$Z_G = \prod_k \sum_{n_k} e^{-\frac{n_k(\hbar \omega_k - \mu)}{k_B T}} \tag{2.3}$$

For a system with a fixed number of bosons N, we can then try to solve for μ. From the partition function the number of bosons per energy level has a mean of

$$< n_k >= \frac{1}{e^{\frac{\epsilon_k - \mu}{k_B T}} - 1} \tag{2.4}$$

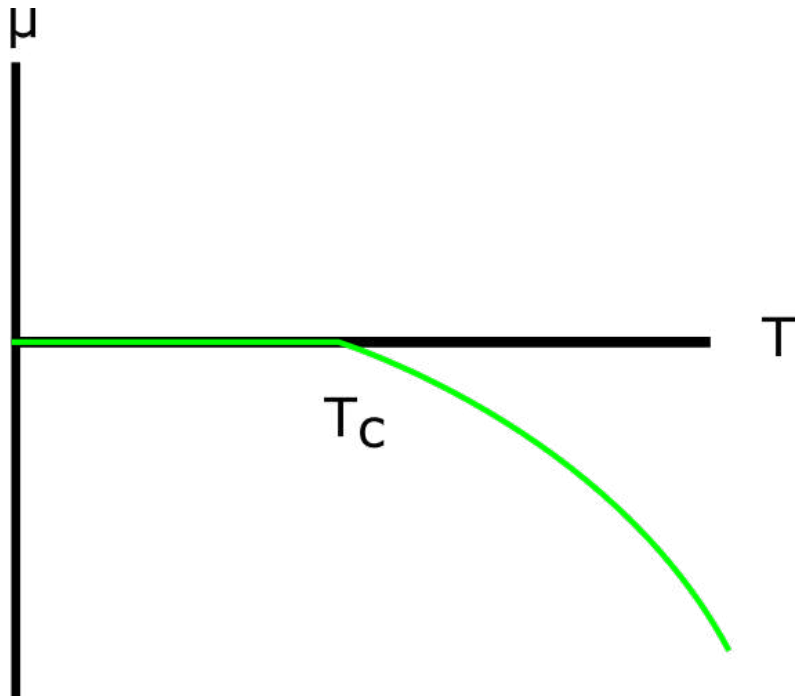

Figure 2-2: Plot of μ vs T. At T_c, μ drops to 0, signifying a phase transition.

so calculating the density then gives

$$\begin{aligned} n &= \int \frac{d^3k}{(2\pi)^3} \frac{1}{e^{\frac{\epsilon_k - \mu}{k_B T}} - 1} \\ &= \int \frac{d^3k}{(2\pi)^3} \sum_m e^{-m(\epsilon_k - \mu)/k_B T} \\ &= \sum_m \frac{z^m}{m^{3/2}} \int \frac{d^3k}{(2\pi)^3} e^{-\epsilon_k / k_B T} \\ &= g_{3/2}(z)/\lambda_T^3 \end{aligned} \tag{2.5}$$

where $g_{3/2}(z) = \sum_{m=1} z^m/m^{3/2}$, $z = e^{\mu/k_B T}$, and $\lambda_T = \sqrt{\frac{2\pi\hbar^2}{Mk_B T}}$ is the thermal wavelength. If we try to solve $n\lambda_T^3 = g_{3/2}(z)$ for μ, we find that when $n\lambda_T^3 > 2.612$, since $g_{3/2}(1) = 2.612$ and is unbounded for $z > 1$, that μ approaches 0 at such densities.

If one calculates the plot of μ over T, you see that there is a significant transition at T_c where μ suddenly vanishes, as seen in figure 2-2. What we see happening is that for $T < T_c$, the approximation used for the integral actually breaks down because a significant fraction of the bosons is present in the ground state, giving what we know

as the Bose-Einstein condensate, and must thereafter be accounted for separately. This temperature can be calculated as

$$T_c = \frac{2\pi\hbar^2}{Mk_B}(\frac{n}{g_{3/2}(1)})^{2/3} = 3.312\frac{\hbar^2 n^{2/3}}{Mk_B}. \tag{2.6}$$

We therefore need both low temperatures and high density to have the necessary conditions for a BEC.

2.2 Degenerate Fermions

While the math is somewhat different for fermions, we find a similar crossover between the classical to quantum picture when fermions approach low temperatures. When at high temperature, we expect fermions to act similar to a non-interacting classical gas. However, as temperature lowers, due to the Pauli exclusion principle, only one fermion is allowed to exists in the lowest energy states, and the point where the quantum and thermal effects are similar, allowing for quantum statistics to dominate, is known as the Fermi temperature.

The partition function is similar except for the fact that there can only be 0 or 1 fermion in each energy level, so we then obtain

$$Z_G = \prod_k (1 + e^{-\frac{\hbar\omega_k - \mu}{k_B T}}) \tag{2.7}$$

$$n_k =< n_k >= \frac{1}{e^{\frac{\epsilon_k - \mu}{k_B T}} + 1} \tag{2.8}$$

From this the pressure in the low temperature limit is calculated to be

$$P = \frac{2}{3}\frac{U}{V} = \frac{3}{5}(3\pi^2)^{2/3}\frac{\hbar^2 n^{5/3}}{2M} \tag{2.9}$$

The Fermi temperature where the classical and quantum description cross over is

given by when the pressures are nearly equal at approximately

$$T_F \approx \frac{\hbar^2 n^{2/3}}{2Mk_B}. \tag{2.10}$$

2.3 BEC in Harmonic Potential

Of course, in actual experiments, we are not working in a box, but in a harmonic potential with the particles interacting with each other. We can instead use field theory to describe the system and obtain equations used to describe the system.

Under field theory, we find that the equation describing the dynamics of the system is given by the Gross-Pitaevskii equation

$$i\hbar\frac{\partial\psi}{\partial t} = \left[-\frac{\hbar^2}{2M}\frac{\partial^2\psi}{\partial x^2} + U(x) - \mu + g|\psi|^2\right]\psi \tag{2.11}$$

where $\int |psi|^2 = N$, U is the harmonic potential, μ is the chemical potential, and $g|psi|^2$ represents the mean interaction between bosons.

We can then take the assumption that the interaction energy is large compared to the kinectic energy and take the Thomas-Fermi approximation to ignore the first term, so that

$$(U(r) - \mu) + g|\psi|^2 == 0 \tag{2.12}$$

for the ground state, giving the approximation of

$$|\psi|^2 = \frac{\mu - U(r)}{g} \tag{2.13}$$

Using the harmonic potential $U(r) = \frac{1}{2}M\omega_0^2$, we find the maximum radius of the BEC to be

$$r_{max} = \left(\frac{15gN}{4\pi m\omega_0^2 r^2}\right)^{1/5} \tag{2.14}$$

. Of course, in the actual experimentation, we observe both the BEC in the center, whose radius is determined by the depth of the harmonic trap, and surrounding thermal atoms. When we detect that the spatial distribution of atoms is not Gaussian

but an inverted parabola, we have then determined to have detected a BEC.

Chapter 3

Trapping and Cooling of Neutral Atoms

It takes a specific combination of density and temperature in order to achieve degeneracy and create a BEC. However, it is arguably difficult to capture and control atoms, small particles on the order of 10^{-10} m, as we cannot possibly physically grab or see them, and single atoms or molecules in the atmosphere are often moving at the order of 600 m/s. In addition, we need to be able to isolate the atoms and prevent unfavorable types of collisions. A variety of techniques are developed to try to control the many possible interactions during collisions. For simplicity, many ultracold experiments utilize alkali atoms because they contain only a single electron in their outermost valence shell, and can thus be approximated as a hydrogen atom with low lying excitations when modeling its energy spectrum [7]. This and the accessibility of electrical excitations with visible and near IR lasers makes alkali atoms attractive for use. However, it is in principle possible to use the electronic structure of any atom or molecules to trap and slow down the desired particles.

3.1 Using lasers to apply force on atoms

We want to have a relatively isolated collection of atoms so that we can control the atoms and their interactions. Since we want to maintain control over the type of

atoms and minimize unnecessary collisions with air molecules and other sources of heating, the experiment would take place in an ultralow vacuum chamber. However, we also want to have a high enough starting number of the target atoms within this vacuum. To achieve this, the method used is to have an oven that heats a sample of the element and have a small nozzle from which the atoms can flow out. Due to the small size of the opening, most of the atoms will flow directly out from the hole through effusion and if stray beams are filtered with a disk containing another small opening, one can create an atomic beam. The next step then becomes to slow down the atoms in the beam to near zero velocity.

3.1.1 Zeeman Slower

For a given atom, we have a collection of energy levels given by the Hamiltonian in a Coulombic potential with fine and hyperfine splitting due to relativistic effects and interactions between spins and orbital angular momentum. Let us consider the collision between the atom at zero momentum and a photon with transition energy $\hbar\omega$ between two levels. When the atom absorbs the photon, it will absorb the momentum, and when the photon is emitted, it goes in a random direction and thus provide an average momentum of zero to the atom. therefore the average momentum on the atom is changed by $\hbar k$, where k is the wavevector of the photon at frequency ω. However, the probability of the photon being absorbed and emitted is dependent on the difference in frequency δ between the photon frequency and the transition energy between states of the electrons, so that the scattering rate is

$$R = \frac{\Gamma}{2}\frac{\Omega^2/2}{\delta^2 + \Omega^2/2 + \Gamma^2/4} \tag{3.1}$$

where Γ is the linewidth of the transition, Ω is the Rabi Frequency of the transition, and δ is the offset of the laser frequency from the transition frequency ω. Thus, given an atomic beam, we would want to optimize the slowdown of the atomic beam by matching the laser frequency to the atomic transition. The atoms, however, will see a different frequency at higher speeds due to the Doppler effect, and thus the scattering

rate and the number of atoms slowed down will drop over time. We thus want to adjust either the photon or the transition energy to obtain a matching frequency at a given speed.

In the Zeeman slower setup, the atoms are placed in a magnetic field, which then perturbs the energy levels through the Zeeman effect and thus adjusts the transition energy to match the given speed. At a speed $v << c$, the Doppler effect states that

$$\omega' = \omega \left(\sqrt{\frac{1+v/c}{1-v/c}} \right) \approx \omega(1+v/c). \tag{3.2}$$

By the Zeeman effect the new transition energy is then given by

$$\omega' = \omega + \frac{\mu_B B(z)}{\hbar} \tag{3.3}$$

where μ_B is the Bohr magneton and B is the magnetic field. If we want constant deceleration of the atoms, we require v as a function of position z to be

$$v = v_0 \sqrt{1 - z/L_0} \tag{3.4}$$

where v_0 is the initial speed and L_0 is the desired length of the Zeeman slower. We then find that we require the magnetic field B to depend on the position along the slower as

$$B(z) = B_0 \sqrt{1 - z/L_0} + B_{Bias} \tag{3.5}$$

where $B_0 = \frac{hv_0}{\lambda \mu_B}$. We thus adjust the magnetic field to match the transition frequency to the laser and slow down the atoms efficiently along the path.

3.2 Magneto-Optical Traps

Once the atoms have been slowed down, we then want to trap them and create a high density, low temperature collection of atoms to approach the conditions necessary for a BEC or degenerate atoms. We can use the fact that light applies a force on the

atoms to slow and trap them.

At the most basic sense, we can simply apply a radiation source along all 3 axis and push the atoms towards the center of the point where they are aligned. If the light is red shifted from the transition frequency when the atom is still, then an atom traveling against the beam at velocity v will see the incoming light as blue shifted compared to the light from behind, causing a gradient and pushing the atoms back to zero velocity. This can be described as an overall damping force

$$F = -\alpha v. \tag{3.6}$$

This, however, does not trap atoms but only slow them down with a a damping force, which allows them to accumulate around the center.

This model can be further improved so that the atoms are not just slowed down but actually trapped in the center by utilizing an inhomogenous magnetic field and circular polarizations of light. Consider a transition from $J = 0$ to $J = 1$, with J as the total angular momentum. If a magnetic quadrupole field is applied using a pair of coils, then the field's magnitude is zero at the center and linear along each direction. This then splits the $J = 1$ energy levels through the Zeeman effect. If the incoming laser beam is redshifted and have opposite polarizations, they excite different transitions in m_J. Therefore, an outgoing atom only feels the incoming beam and is therefore pushed back to the center. Since the Zeeman effect increases as B increases away from the center, the strength of the increasing beam increases the further the atom is away from the center as the lowest energy level gets closer to the laser's frequency, giving an overall force in the form of

$$F = -\alpha v - \frac{\alpha\beta}{k}x \tag{3.7}$$

where k is the photon wavevector, α is the damping constant, and β is the gradient of the transition frequency over distance from Zeeman effect.

One issue that has to be dealt with for some MOTs is that as atoms are repeatedly excited and decayed, due to their hyperfine structure it is quite possible for them to

decay to a different and lower energy level through spontaneous emission, making them no longer accessible to excitations with the trapping light. To improve the efficiency of the trap, we would then need to add an additional transition to excite the atoms in the trapped state back into the cycle, which is known as a repump light.

Putting these ingredients together makes what is known as a MOT. With this a large number of atoms can be trapped at high density. It is, however, not completely sufficient to simply trap the atoms to achieve a BEC. Due to interactions with the photons due to absorption and spontaneous emission, there still remains a limitation called the Doppler cooling limit, which prevents the energy from going below $k_B T = \hbar\Gamma/2$. While other optical methods exists to go below this limit, such as Sisyphus cooling, there still exists a recoil energy from spontaneous emission of the photons that prevents further cooling. Other steps needs to be taken.

3.3 Optical Dipole Trap

In contrast to the MOT, which utilizes the scattering force, optical dipole traps instead uses the dipole force. A simple image to understand this force is to consider light refracted through a triangular prism. Even though the momentum of light is the same coming in and coming out, the fact that the light had changed direction implies that momentum had been transferred from the light beam to the prism, enacting a force upon it. Therefore the simple refraction of light through a particle allows it to interact with the particle.

A full expression for the force acting upon a particle can be given by

$$F = \frac{\hbar k \Gamma}{2} \frac{\Omega^2/2}{\delta^2 + \Omega^2/2 + \Gamma/4} - \frac{\hbar \delta}{2} \frac{\Omega}{\delta^2 + \Omega^2/2 + \Gamma/4} \frac{\partial \Omega}{\partial z} \tag{3.8}$$

where the first term represents the scattering force and the second term the dipole force. Here k is the photon wavevector, Ω is the Rabi frequency, Γ is the transition linewidth, and δ is the detuning of the laser from the transition frequency.

To enact such a trap, one uses a singular beam at high intensity that is far from

a resonant frequency at high power. This eliminates the presence of the scattering term and, if the power is high enough, allows for the interaction to be dominated by the dipole term. Thus one can trap atoms using a single laser at high enough power.

3.4 Optical Lattice

Sometimes we need to create a lattice of atoms, which can be useful for trapping and for modeling condensed matter systems under a lattice model. The optical lattice utilizes the concept of the optical dipole trap to create a series of repeating well potentials. If you send a beam in and retroreflect it, you can create a standing wave upon which the alternating points of high and low intensity radiation exists. The atoms are then attracted to the regions of highest intensity under the same principles through which the optical trap works. Trap depth can then be controlled through the laser intensity and the specific frequency used to make the well.

3.5 Magnetic Trapping

Once temperature is low enough, it is quite possible to trap the atoms using only a magnetic field if you have a low field seeking state. Since the atoms are neutral, their energy are most dependent on the kinetic energy and the term $H_{zeeman} = -g_F \mu \cdot B$,which describes how a magnetic dipole interacts with the field, where g_F is the g-factor and μ is the dipole moment. If g_F is positive, when the angular momentum is positive, giving a negative projected dipole moment μ_m in the direction of the B-field, the atom will tend to adiabatically seek the area of the magnetic field where the field is of lowest magnitude to minimize this interaction energy. If the temperature is low enough, a quadratic trap can be made using pairs of coils, keeping the atoms inside.

3.6 Evaporation

We now have a large number of atoms trapped and interacting thermally in a magnetic or optical trap, and we wish to try to reduce the temperature even further without using photons that could heat the temperature further. One way to do this is by eliminating the highest energy particles and letting the atoms rethermalize, just like blowing the steam off of a cup of coffee. This is known as evaporation [8].

The idea here is that, in a harmonic potential, atoms pile up from the lowest energy state in the middle of the trap to the edge where $U(r_{max}) = \mu$, where μ is the chemical potential, and start to spill over where the energy is highest. The difference in magnetic strength implies a difference in resonant energies, thus you can detect and measure the highest energy atoms with rf-spectroscopy. If you then apply the frequency for the highest energy atoms and sweep towards the frequency for the lowest energy ones, you can excite and kick out the highest energy atoms by exciting the hyperfine state transitions at the edge of the trap. If the atoms are then able to rethermalize among all 3 axes, we are then left with a concentration of atoms that average to a lower temperature. This does inflict a loss in atom counts, but if the rate of loss is low enough, the conditions may be met such that a BEC then forms.

3.7 Sympathetic cooling

Sometimes it is not possible to use evaporative cooling or another direct method to further lower the temperature of the sample due to too great of a loss rate or too small particle count. In this case, we want to allow collisions between the atoms and another gas, one that is at a lower temperature. This is known as sympathetic cooling, and is used to lower the temperature of fermionic atoms such as ^{6}Li. Care however needs to be taken to ensure that chemical reactions do not also occur that can release thermal energy and thus cause a loss of more particles.

Chapter 4

Feshbach Resonance

Feshbach resonance is a phenomenom originally studied in nuclear systems and then later studied in collisions of atoms at low temperature. The idea behind this is that when two low temperature particles collide, it is possible to be in resonance with a bound state that can be acted upon. In terms of atomic physics, this means that when the energy of the unbound atoms approaches the energy of a bound molecular state and combine, it is possible for a quasi-bound molecule to momentarily form during collisions. Once this excited Feshbach molecule is formed, it is quite possible to then to use lasers to change the state of the molecule down to its ground state, which then creates a stable bound molecule [9].

4.1 Feshbach Molecules

Let us first construct the model upon which we develop the formalism to understand this. Let there be two molecular potentials $V_a(r)$ and $V_b(r)$ for a pair of atoms within a magnetic field, as seen in figure 4-1, and assume that the total energy of the incoming atoms are slightly above V_a. These potentials correspond to molecules with different configurations of spins when far apart. At the asymptotes, the two potentials approach the energy of unbound atoms with zero kinetic energy. We name the lower potential $V_a(r)$ as the open channel, the state in which the atoms come in and from which a molecule can spontaneously come apart, and $V_b(r)$ the closed

channel which is normally inaccessible and for which the molecule would stay bound at the given energy. The difference between the unbound atomic states comes from both the hyperfine splitting of the particle and the difference in magnetic moment giving a differential Zeeman shift, so if one tunes the magnetic field, they can adjust the difference between the spin potentials in a given magnetic field, given by

$$H_{int} = -\frac{\mu_B B_z}{\hbar}(g_L L_z + g_S S_z) \tag{4.1}$$

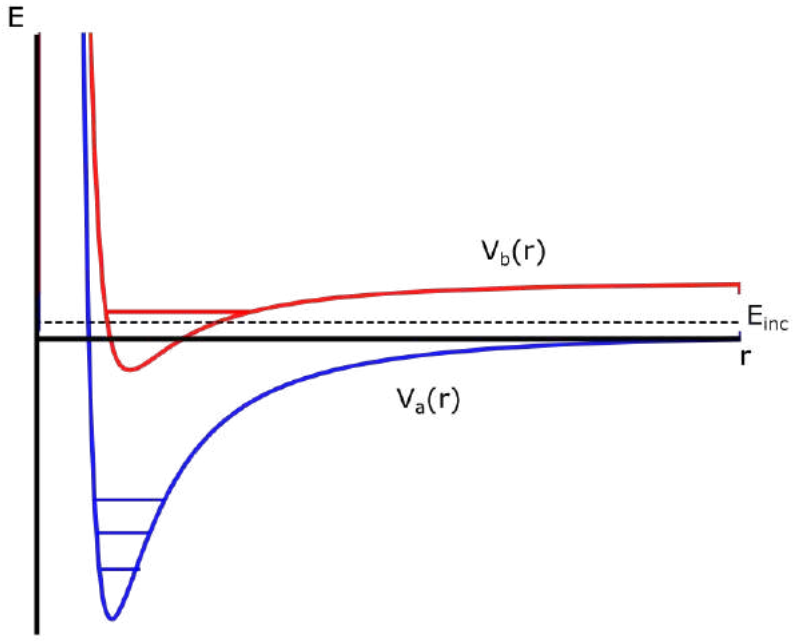

Figure 4-1: When the energy of the incoming atoms in a collision matches that of a bound or quasi-bound state as shown, the two states become mixed together.

4.2 Formalism

Let us describe this system using scattering theory. We will be using a Hamiltonian for the overall system given by

$$-\frac{\hbar^2}{2\mu}\frac{\partial^2\phi}{\partial R^2} + V_l\phi = E\phi \tag{4.2}$$

where $\phi = \psi/R$ is the radial wave function. Thus if one has an incoming plane wave of momentum k, the whole solution can be described as the sum of the incoming wave and reflected spherical waves of the form

$$\phi = \frac{c}{\sqrt{k}} \sin kR - \pi l/2 + \eta_l(E) e^{i\eta_l(E)} \tag{4.3}$$

where η determines the significant properties of the collisions.

Ultracold collisions work in the regime where $k \to 0$ so we can use the lower limit approximations of the solutions, which are given for the s-wave by

$$\tan \eta = -ka \tag{4.4}$$

where a is the s-wave scattering length. An expansion of this equation is given by

$$k \cot \eta(E) = -\frac{1}{a} + \frac{1}{2} r_0 k^2 \tag{4.5}$$

where r_0 is defined as the effective range of the potential.

To fully describe the interactions, we define the cross section as

$$\sigma_e = g \frac{\pi}{k^2} |1 - S(E)|^2 \tag{4.6}$$

for elastic collisions and

$$\sigma_i = g \frac{\pi}{k^2} (1 - |S(E)|^2) \tag{4.7}$$

for inelastic collisions, where $S(E) = e^{2i\eta_l(E)}$ and g is the g-factor depends on the statistics of the particles, with $g = 1$ if distinguishable. If there are multiple channels, we can then define a complex scattering length $\tilde{a} = a - ib$ to allow S to be non-unitary. Then the elastic cross section becomes

$$\sigma_e = 4\pi g(a^2 + b^2). \tag{4.8}$$

Of course, this solution is separate to any existing bound-state solution. To differ-

entiate, we define the scattering wave solution as $|E\rangle = \phi_{bg}|bg\rangle$ and the bound state solution as $|C\rangle = \phi_c|c\rangle$, where $|bg\rangle$ and $|c\rangle$ encode the angular momentum degree of freedom. E is the energy of the incoming plane wave and E_c is the energy of the bound state from its own potential.

4.3 Resonance and scattering length

To describe resonance, we need both the scattering picture and the bound state to be present. The resonance comes about because there exists a term within the Hamiltonian, denoted as $W(R)$, that encourages intermixing between the two sets of solutions. We can then describe the new phase shift as $\eta = \eta_{bg} + \eta_{res}$ where η_{bg} is the portion that comes about solely from the potential V_a for the incoming atoms and η_{res} comes from the interaction between the free and bound potentials. This can be described by

$$-\tan\eta_{res} = \frac{\frac{1}{2}\Gamma(E_c)}{E - E_c - \delta E(E_c)} \tag{4.9}$$

Here, Γ is the width of the resonance given by

$$\Gamma = 2\pi|\langle C|W(R)|E\rangle|^2 \tag{4.10}$$

which, when $k \to 0$, is given by the limit $\Gamma = ka_{bg}\Gamma_0$. δE is given as the second order perturbation of the bound state solution due to the mixing term $W(R)$, given by the principal integral

$$\delta E = \int_{-\infty}^{+\infty} \frac{|\langle C|W(R)|E'\rangle|^2}{E - E'} dE', \tag{4.11}$$

allowing us to define a new energy for the bound state as $E_0 = E_c + \delta E$.

Using these definitions, we can define the new complex scattering length to be

$$a = a_{bg} + \frac{a_{bg}\Gamma_0}{-E_0 + i\gamma/2} \tag{4.12}$$

where $\gamma/\hbar$ is the decay rate, which is mostly insignificant for magnetic feshbach resonance.

By defining $E_c = \delta\mu(B - B_0)$ to describe the energy dependence of the bound state, we can then define

$$a = a_{bg}\left(1 - \frac{\Delta}{B - B_0}\right) \tag{4.13}$$

where $\Delta = \Gamma_0/\delta\mu$. From this equation, we can see that as B approaches the crossover resonance, we see a sudden increase in the magnitude of the scattering length, which can then be used to control interactions between particles.

4.3.1 Describing Resonance strength

By using a unitless description of the equations, we can then obtain a dimensionless parameter describing the Feshbach resonance, which can then be used to describe different behaviors as the threshold is crossed. For the Van der Waals potential

$$V = -\frac{C}{r^6} + \frac{\hbar^2}{2\mu}\frac{l(l+1)}{r^2} \tag{4.14}$$

we can define the mean scattering length

$$\bar{a} = \frac{2\pi}{\Gamma(1/4)^2}(\frac{2\mu C}{\hbar^2})^{1/4} \tag{4.15}$$

and the energy scale

$$\bar{E} = \frac{\hbar^2}{2\mu\bar{a}^2} \tag{4.16}$$

.

We can then define a dimensionless parameter

$$s = \frac{a_{bg}}{\bar{a}}\frac{\delta\mu\Delta}{\bar{E}} \tag{4.17}$$

where a_{bg} is the background scattering length. In the case where $E \to 0$, the resonance width $\Gamma(E)$ and the energy shift δE are both shown to be proportional to $\bar{E}s$.

There are two cases to describe. When $s >> 1$, the resonance is broad or entrance-channel dominated. In this case a large fraction of the width can be described using the model above and the resonant states have much of the spin characteristics of the

entrance channel. In contrast, when $s << 1$, the system can only be described as such for a small fraction of the linewidth near $B = B_0$. A significant impact is that the fraction of the bound state is near 1 for a large part of the resonance in the narrow resonance.

4.4 Resonance and state mixing

There are differences in the mixing behavior depending on whether the Feshbach resonance is broad or narrow. For a broad resonance, since the state stays in the universal regime for a large fraction of the resonance width Γ, there is a preference of the atoms staying unbound for most of the transition and is well approximated by 4.13, which is useful for controlling the scattering length. In contrast, for narrow resonances this approximation breaks down within a short range of B_0 compared to the linewidth, which implies a faster drop in the number of unbound atoms as resonance is crossed. This can be seen in the image above in figure 4-2, which comes from [9]. As this graph demonstrates, for broad resonances, the fraction of molecules remain low for most of the transition until far past the resonant point, at which all the atoms turn into molecules, while for the narrow resonance, the atoms quickly all turn into Feshbach molecules with nearly 100% transition efficiency as it crosses the resonance. In both cases, we see variability in the scattering length and that the process eventually creates Feshbach molecules as the B-field crosses the resonance into negative scattering lengths, which can then be further used to create more stable molecules, as discussed in the next chapter.

4.5 Utility of Feshbach Resonance

From this discussion, we can understand a variety of properties in Feshbach resonances that can be used for scientific purposes. The main one is the manipulation of the scattering length. Looking again at figure 4-2, we see that, if the scattering is described, one can increase the scattering length to large values, allowing for increased

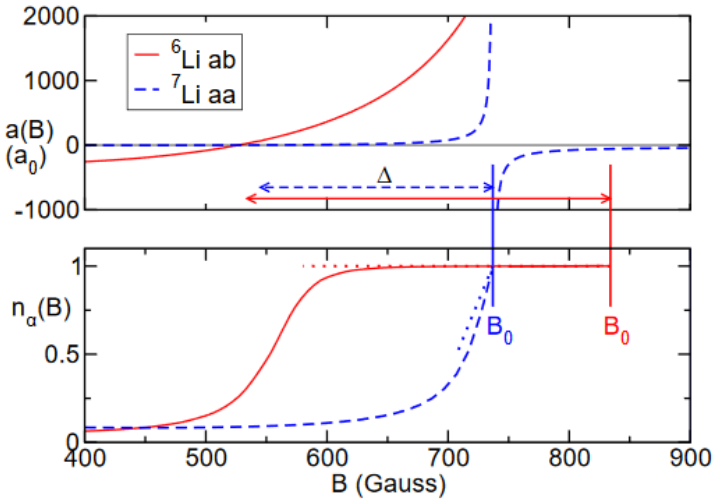

Figure 4-2: The first plot depicts the scattering length of a narrow (blue) and broad (red) Feshbach resonance, and the second plot contains the fraction of uncoupled atoms as B is ramped down, showing that they all drop and convert to molecules. The plot comes from [9].

repulsive interactions that can impact scattering dynamics. One can also reduce the scattering length to zero, forcing short range interactions to be dominant, or allowing it to be less than zero allows for strong attractive interactions and, for fermions, the formation of Cooper pairs and other interesting phenomena.

Of course, being able to utilize Feshbach resonances for scientific purposes require a knowledge of what resonances exists, their attributes, and how to control them. Much of it depends on the width and strength of the resonance and how reasonable it is to achieve the required magnetic strength. As such, plotting the spectrum of atoms is useful for determining where we may expect resonant states and its quality, as well as describing the energy spectrum of the atoms.

For some atoms, it can be difficult to calculate the Feshbach resonances explicitly. Consider Dysprosium, an atomic element with very high magnetic moment. Due to the complicated nature of the atomic energies, the energy spectrum of its dimer is said to be dependent on random fluctuations and thus considered to be chaotic. As such, it is considered to be an example of quantum chaos and difficult to analyze. It is, however, possible to use random matrix theory to give a general description of

the energy spectrum. Depending on whether the energy levels are weakly or strongly interacting, one may be able to observe either a Poissonian or Wigner-Dyson distribution, which can be seen when you measure the spectrum of Feshbach resonances [10]. The same story is true for determining the energy levels of complex molecules.

On the other hand, as seen with the lower part of figure 4-2, crossing over the resonance to where the scattering length is negative allows for the creation of weakly bound molecules, which can then be manipulated into lower energy, more strongly bound molecules using optical methods, as seen in the next chapter. This still requires characterizing the Feshbach resonance to know the field strengths at which molecules are formed.

In either case, it becomes critical to understand and control the magnetic field to be able to control the scattering length and utilize magnetic Feshbach resonance to efficiently create molecules and bound states. This is why, for the more narrow and sensitive resonances, it is important to minimize magnetic noise as much as possible for control and efficiency. Therefore it is of interest to eliminate background noise and eliminate any non-intentional DC fields in the environment to ensure that the Feshbach molecule state is stable.

Chapter 5

STIRAP

Many problems exists for producing low-temperature molecules by direct cooling methods. First, the complex energy level structure makes it difficult to control the state of the system for laser cooling. In addition to the energy structure of a multi-electron body within a polar or non-symmetrical body being non-trivial, the nuclei themselves stretch and vibrate, giving rovibrational substructures that increases the complexity and further complicates the system. This complexity also makes understanding the collisional dynamics of molecules an even more difficult task than it already is, as new chemical reaction channels may provide new and unintended consequences. Even the most simple molecules have energy structures and collisional dynamics difficult to analyze computationally, which drives some of the motivation towards developing quantum computers [11].

In addition, even when the energy levels are understood to allow for the correct selection of lasers for cooling, direct cooling has proven to be a difficult task. Various groups have worked on direct cooling of molecules but the temperature has still been limited to over 20 μK experimentally and the density has still been too low to shift the molecules to degeneracy [12][13][14]. Thus, with the goal of producing degenerate molecules, various researchers have turned to directly assembling the molecules from ultracold atoms to ensure that the molecules remain at low temperature.

With Feshbach resonance, we see that the atoms enter a bound state at certain magnetic field strengths. These molecules, however, are at an excited state and can

easily collide, break apart, and cause the atoms to escape the trap at high velocity, leading to loss in the number of molecules and reducing the density. This making it impossible to achieve degeneracy with just these molecules. To counteract this, we would need to transfer the molecules from an excited state to a lower energy ground state that would be stable and not bound to break apart before any attempt can be made at further cooling.

One straightforward way of doing this is to apply a Rabi oscillation between the energy state, which uses a timed pulse of a single oscillatory field to excite the population of atoms from one state to another. By exciting the transition between states, the molecules should rotate from one state to another periodically, just like how one would rotate the spins of a qubit. However, this method is inefficient at converting the molecules to the ground state, for reasons discussed in 5.1.1.

A more efficient manner to producing stable molecules from Feshbach molecules is to instead utilize STIRAP, or Stimulated Raman Adiabatic Passage, which adiabatically transfers the molecules from the initial state to a dark state orthogonal to a third excited state created using radiation before moving it down to the ground state. This has been used to adjust the energy level of the molecule with very high efficiency, as it has been used jointly with Feshbach resonance within the lab to produce fermionic NaLi molecules [4].

5.1 Rabi Oscillations

We first use Rabi oscillations to explain the interaction between energy levels with photons and demonstrate a model that can be extended for STIRAP.

Let us consider a two level system with the excited state $|e\rangle$ and ground state $|g\rangle$ with energy gap $\hbar\omega$, perturbed by an oscillating electric field of frequency ω_L. The Hamiltonian is then given by

$$H = H_0 - \vec{d} \cdot \vec{E} \tag{5.1}$$

where $d = \langle \psi_i | \vec{r} | \psi_j \rangle$ is the dipole moment operator, which can be nonzero only when ψ_i and ψ_j are not equal due to their opposite polarity. If we define $\vec{E}(t) = \vec{E} e^{i\omega t}$, and

$\vec{d}_{eg} = \langle e|\vec{r}|g\rangle$ then we have

$$\begin{aligned} H =& \frac{\hbar\omega}{2}|g\rangle\langle g| + \frac{\hbar\omega}{2}|e\rangle\langle e| \\ & - \hbar(\Omega e^{-i\omega_L t} + \Omega' e^{i\omega_L t})|e\rangle\langle g| - \hbar(\Omega^* e^{i\omega_L t} + \Omega'^* e^{-i\omega_L t})|g\rangle\langle e| \end{aligned} \tag{5.2}$$

where $\Omega = \vec{d}_{eg} \cdot \vec{E}/\hbar$ is the Rabi Frequency and $\Omega* = \vec{d}_{eg} \cdot \vec{E}^*/\hbar$.

If we then perform a unitary transformation under the interaction picture by adding the evolution of each unperturbed state over time, the perturbation then becomes

$$H_1 = -\hbar(\Omega e^{-i(\omega_L-\omega)t} + \Omega' e^{i(\omega_L+\omega)t})|e\rangle\langle g| - \hbar(\Omega^* e^{i(\omega_L-\omega)t} + \Omega'^* e^{-(i\omega_L+\omega)t})|g\rangle\langle e| \tag{5.3}$$

We can then average over short time scales to ignore the high frequency term under the rotating wave approximation and, assuming $\omega_L = \omega$, get

$$H_1 = -\hbar\Omega|e\rangle\langle g| - \hbar\Omega^*|g\rangle\langle e|. \tag{5.4}$$

Under the Bloch sphere picture, this Hamiltonian gives an evolution equivalent to a rotation around the x-axis with the Rabi frequency Ω, as seen in figure 5-1. By performing a π-pulse rotation around the x-axis, we then shift the molecule from E_1 to E_2 and vice versa, thus transferring the particles to the excited state.

5.1.1 Complications of Rabi Oscillations

There are, however, a variety of complications that come about when attempting to use Rabi oscillations to transform a population of atoms or molecules. First, the efficiency of Rabi oscillations is impacted by the frequency of the incoming light. The model above assumed that $\omega_L = \omega$, but if they differ, they introduce a term Δ between the two energy levels. In the Bloch sphere picture, this means that we are no longer rotating around the x-axis, but around a vector slightly above or below, which reduces the number of particles that transitions to the new ground state.

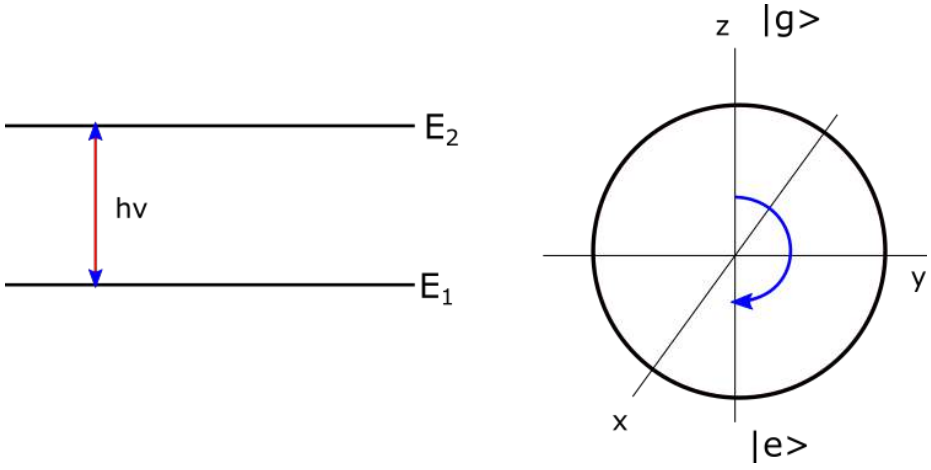

Figure 5-1: Depiction of Interaction in Rabi oscillation on the left and the Bloch sphere picture of Rabi oscillations on the right.

A second complication comes about in the fact that you need precise timing to get complete transfer of atoms. You need to ensure that a π-pulse at the transition frequency is applied to get full transfer, but that timing is difficult to measure, and its not even feasible to provide a square pulse of radiation. Even if the optimal pulse shape is applied, due to thermal effects and differences in the magnetic field shifting energy levels, there may still be decoherence which further reduces the number of transferred atoms. In addition, since the Rabi frequency is proportional to the E field amplitude, you also needed sufficient laser intensity control to have consistent timing requirements. It would be far better to have a method that is not so dependent on having the correct intensity and pulse timing requirements. This is where STIRAP comes in.

5.2 STIRAP

To understand STIRAP, let us begin with a three-level system and its Hamiltonian, linked by radiation coupling between the energy levels as shown in figure 5-2. State 1 is the initial state, state 2 is the coupled excited state, and state 3 is the desired ground state. Two lasers are applied at energies that are offset from the transition energies, with the Pump laser between 1 and 2 offset by Δ and the Stokes Laser

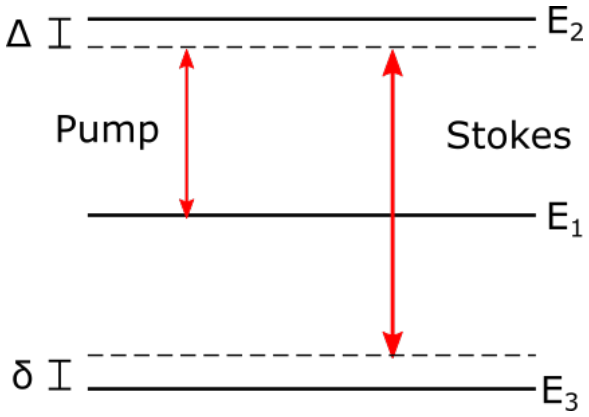

Figure 5-2: Energy levels and interactions in STIRAP.

between 2 and 3 offset by δ. Using the same rotating wave approximation as for the Rabi oscillations, we find that the Hamiltonian describing the interaction between the states can be described by

$$H = \hbar \begin{bmatrix} 0 & \frac{1}{2}\Omega_P & 0 \\ \frac{1}{2}\Omega_P & \Delta & \frac{1}{2}\Omega_S \\ 0 & \frac{1}{2}\Omega_S & \delta \end{bmatrix} \tag{5.5}$$

where Ω_P is the Rabi frequency between states 1 and 2, Ω_S is the Rabi frequency between states 2 and 3, and Δ and δ are the two detuning parameters.

When $\delta = 0$, one of the eigenvalues becomes 0, with the corresponding eigenstate being

$$\Psi_0 = \psi_1 \cos\theta - \psi_3 \sin\theta \tag{5.6}$$

where θ is given by $\tan(\theta) = \Omega_P/\Omega_S$. This is the dark state that does not interact with the incoming radiations. The other two eigenstates are mixed with the excited energy state ψ_2 with

$$\Psi_1 = \psi_1 \sin\theta \sin\phi + \psi_2 \cos\phi + \psi_3 \cos\theta \sin\phi \tag{5.7}$$

$$\Psi_2 = \psi_1 \sin\theta \cos\phi - \psi_2 \sin\phi + \psi_3 \cos\theta \cos\phi \tag{5.8}$$

where $\tan 2\phi = \frac{\sqrt{\Omega_P^2+\Omega_S^2}}{\Delta}$. We thus see that if we adiabatically adjust the mixing angle

θ by adjusting the amplitude of the coupling radiation, we can move the states of the particle from state 1 directly to state 3 without moving it to state 2 where it may decay to other states [15].

5.3 STIRAP Procedure

To perform STIRAP, the procedure then goes as following:

1. Apply a strong Stokes laser between state 2 and 3 to link the two and significantly increase Ω_S.

2. Gradually increase the Pump laser between states 1 and 2 to adiabatically move the molecule from the Feshbach state ψ_1 to the dark state.

3. Gradually reduce the Stokes laser to 0 so that the dark state moves to ψ_3.

4. Ramp down the Pump laser to decouple the states.

When this is done, we find the final state of the molecule to be in the ground state. Of course, this is with the assumption that the Feshbach molecules remain in a bound state during the transition, which is why a sufficiently stable B-field is required.

Chapter 6

Apparatus

A lot of the difficulties that arise in ultracold experiments come from noise in the system, whether that is from lasers, electronics, or magnetic fields. As can be seen from the previous chapters, stable magnetic fields are a requirement for performing sensitive experiments, whether it is to have enough resolution to perform a Feshbach spectroscopy and find the narrow peaks [10] or it is to keep the Feshbach molecule state stable enough to efficiently perform STIRAP and make molecules [4]. Most electronics work toward eliminating as much current and magnetic field noise produced by the system itself, but often ignore the environmental fields around it. As such, the rest of the thesis will discuss the project towards canceling out such noise.

6.1 Strategy

There are two main difficulties in zeroing the magnetic field. First, the experiments occur in a low-pressure vacuum chamber to minimize collisions of the atoms and molecules of interests with other molecules from the air. As such, if not already accounted for, there is difficulty with measuring the magnetic field from within the chamber, making it uncertain what the magnetic field is actually like inside.

Second, when running the experiments, often very strong magnetic fields on the order of multiple Gausses are present for trapping and manipulating molecules. This can easily saturate the magnetometers available to us. While there exists other mag-

netometers that can measure such large fields, they have lower resolution, and we primarily wish to understand and remove the AC environmental fields. Therefore we need a setup that can be installed outside of the vacuum chamber while also having enough resolution to detect and cancel the AC fields.

Previous work had already been done to determine that two magnetometers on the two sides of the chamber is sufficient to estimate the overall value and fluctuations of the magnetic field of the inside of the chamber. This strategy does leave an offset value in the average, but this is independent of any fluctuations in the magnetic field and depends only on the field's curvature between the magnetometer. As such, the offset can be accounted for and tuned out of the magnetic field when optimized.

To cancel the AC fields, we assume that the magnetic field remains approximately periodic during the run time of the experiment. Since the AC fields consists primarily of the 60Hz AC lines and higher harmonics, this is approximately true. We will first record the waveform of the environmental field before running the experiment. This will hopefully be consistent during the experimental run. To deal with the slight variations in the actual frequency, we will use the 60 Hz power lines themselves as a trigger to determine the timing of the output waveform, thus maintaining the signal's integrity. Before turning on the magnetic coils, we then send a trigger to stop recording and to continue playback of the recorded field. This playback can then be adjusted digitally to account for the transfer function of the current driver, the coils, and curvature in the field. The output waveform should then cancel the magnetic field if parameters are tuned correctly.

6.2 Implementation

To implement active feed-forward, we use two magnetometers to cancel the magnetic field, an Arduino micro-controller to record, transform, and playback the magnetic field, and output the voltage to a current controller. We used two Bartington 690-300 Low-Cost Magnetometer to record the magnetic fields and one Bartington 690-100 Magnetometer to probe the center of the region for which we wish to test. To have

enough memory to record data for 3 arrays and the script, as well as a sufficient sampling speed, we decided using the Arduino Due, which has 512 Kb flash memory and a maximal clock speed of 84 MHz. The Arduino setup is connected to an external DAC and ADC to read the magnetometer's voltage and to output a signal to the current controller. In addition, a wall transformer is connected to an outlet and modified using a voltage divider and a NAND schmitt trigger gate to produce a 60 Hz square wave for timing. Before any other magnetic field is turned on, a TTL is connected to the Arduino to tell it to transform the signal that it is reading and produce the output wave. The apparatus is described in figure A-1.

6.3 Communicating with External Apparatus

One issue that came up when attempting to implement this setup is the issue of resolution. To record and output both the AC and DC field, we realized that we needed a resolution of at least 14 bits to measure down to 1 nT resolution while measuring Earth's DC field at 65000 nT without saturation. However, the Arduino only had a 12-bit input resolution, 8-bit output resolution and contained only 2 DAC ports, while we need to be able to record and cancel in all 3 axes. Therefore, we needed to interface with an external Analog-to-Digital Controller (ADC) and Digital-to-Analog Controller (DAC) with sufficient resolution and sufficient speed to accurately record the periodic waveform. This was done using SPI communication.

For the ADC we chose the ADS131A04EVM Board with 4 input channels and 24-bit resolution. It already contained the circuitry for powering the board through USB and for reading the inputs, so we simply installed it directly to the Arduino's SPI port. We chose the settings so that 16-bit inputs were read and the sampling frequency was maximized.

For the DAC we chose the LTC2664 Demonstration board, which also contained 4 output channels and had a 16-bit resolution.

We decided to interface communication using the Serial Protocol Interface (SPI) because it could handle a very fast transfer speed limited only by the clock frequency,

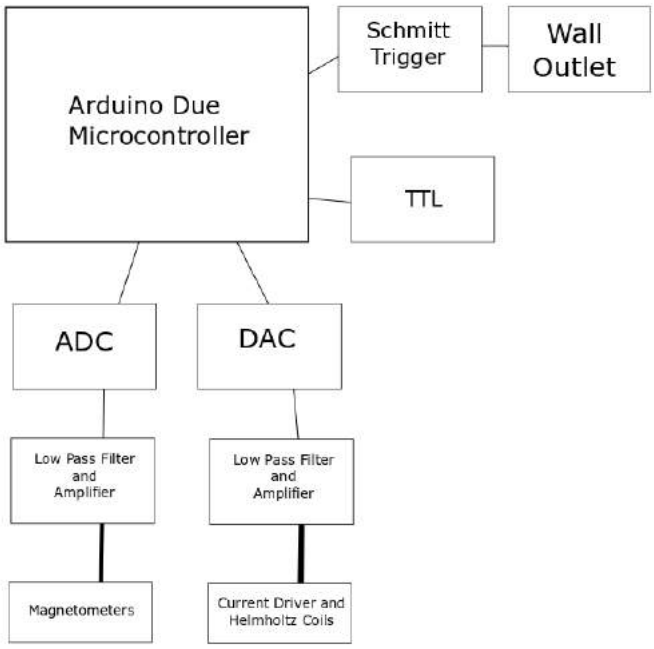

Figure 6-1: The overall setup for all components of the feedforward apparatus.

word length, and physical hardware. In addition, the Arduino Due contained libraries for communicating using SPI and dedicated pins. Details on how this works and specific settings for the devices are in Appendix A.

6.4 Circuit

The circuitry for the setup is described in figure 6-2. For each channel, we average the magnetometer signal and adjust the gain so that it is within the 3.3V range of the ADC, filter out the 15 kHz noise from the magnetometer's switching frequency and any other high frequency sources, and connect to the ADC's input. That signal is the communicated to the Arduino through SPI, which then records the signal and communicates the new voltage with the DAC. The DAC then sends the voltage to an amplifier to modify gain and a filter to remove high frequency noise over 15 kHz.

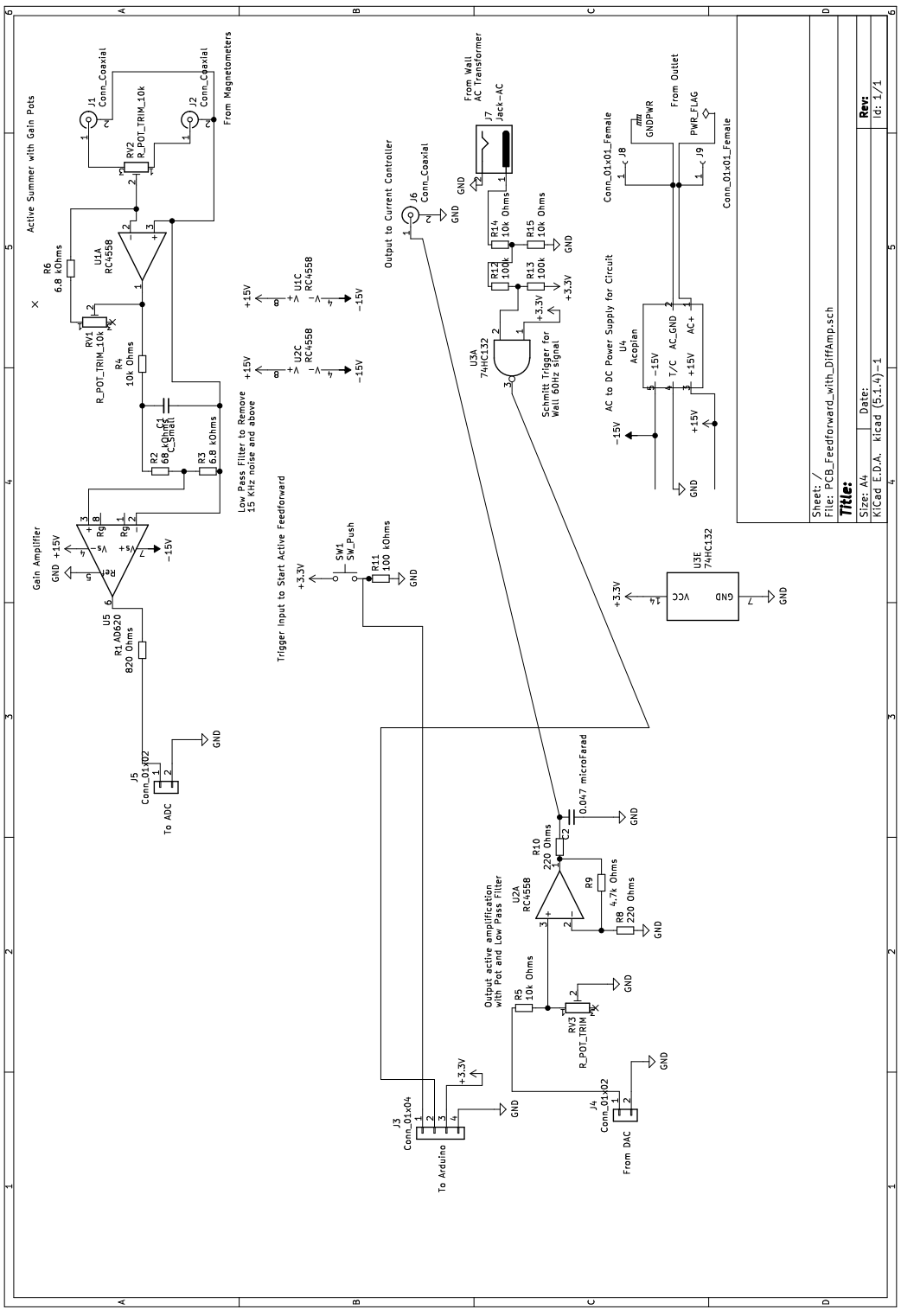

Figure 6-2: Schematic for the Arduino circuit.

6.5 Testing Environment

To test the apparatus, we constructed a test chamber using 80/20 aluminum bars and insulated copper wire. We constructed the box to be a cube of dimensions 30.5 cm x 30.5 cm x 15.5 cm to mimic the actual chamber we expected to use.

The coils were of a gauge of 30 AWG. We wrapped the coils seven times around the edges of the square faces so that it formed a Helmholtz coil configuration. We then connected the coils to the current controller. The inductance of the coils was calculated to be about 132 μH.

The current was provided through an in-house built current controller designed by Michael Cantara and powered by a BK Precision 1688B power supply. This current controller measures the current using a 0.01 Ω sensing resistor and utilizing a PI feedback loop to control current.

To place the magnetometers, we first put one magnetometer in the center and ran the magnetic coils. We adjusted the position of the magnetometer, moving along the axis of the coils, until the field being measured from the coils were maximal. We then placed the two other magnetometers on the side at a distance of 8 cm away from the edge of the chamber. The overall setup can be seen in the picture in figure 6-3.

6.6 Algorithm

The algorithm follows the flow as described here. The Arduino initializes both Serial and SPI communication and initializes all matrices. It starts by recording a single set of measurements until it receives a 60 Hz trigger signal from the wall connection.

It then enters a Recording mode where the Arduino saves the measurements it receives from the ADC and alternates saving between two arrays, switching after two trigger signals. When saving into one array, it sends to the DAC the value from the other array. This continues until it receives a TTL signal to tell it to stop recording and playback the signal in Halt mode.

When it first enters the Halt mode, the arduino takes the array that was not cut

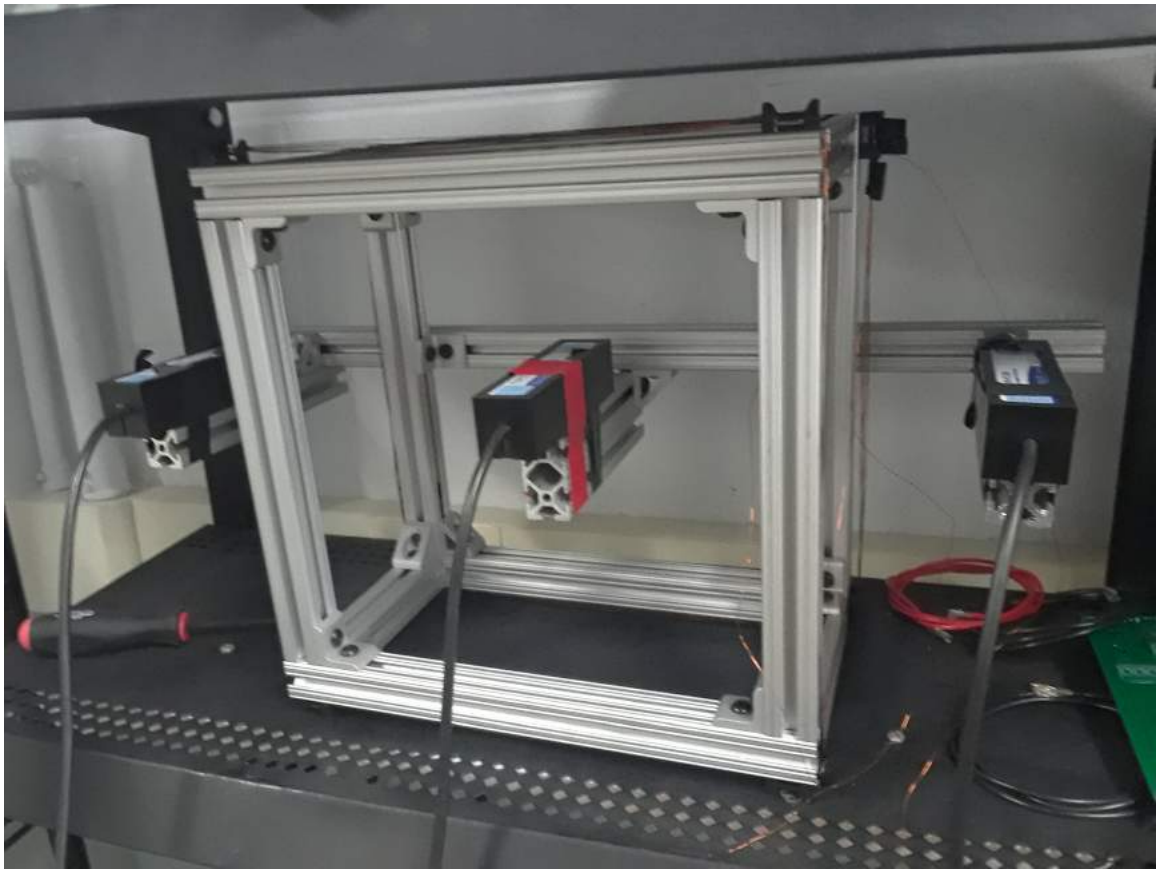

Figure 6-3: The testing chamber is shown above.

off by the TTL, as it represents two full cycles. The number of samples is nearly constant per run at 236 samples per cycle, so we assume that there are 236 samples per cycle that need to be outputted. We resample and interpolate the data so that we have 512 data points over 2 cycles, then perform an FFT. We adjust the phase and magnitude of the 0, 2, 6, and 10 data points and corresponding conjugate in the Fourier Transform to adjust the DC, 60 Hz, 180 Hz, and 300 Hz components of the signal and set all other points to zero to eliminate noise caused by spikes in the input signal. We then perform an inverse transform to obtain the adjusted waveform.

We then repeat the steps performed when recording, except we save the ADC value to a dummy matrix and output to the DAC. The steps are repeated to ensure that the sampling frequency is equivalent for the data collection and data output. This continues until the TTL signal is dropped, at which point we start recording again.

Chapter 7

Results

7.1 Performance

Since the apparatus is on a test chamber, we would like to characterize its behavior to ensure that it is capable of canceling the field by evaluating the noise being canceled, the apparatus's performance in doing so, and its ease of control.

7.1.1 Noise measured in the environment

First, we would like to characterize what noise exists in the environment. The main source of environmental magnetic fields comes from the Earth's magnetic field, but this tends to be static on long time scale. The main source of noise that we expect are to be electrical noise from power lines, which run at approximately 60 Hz. We thus want to ensure that the field is mostly consisting of the 60 Hz components and its harmonics.

We can do this by measuring the bare magnetic field input and measuring the Fourier Transform of the signal transfer function. This is seen in figure 7-2. In this plot, the DC component has been cut off so that the other frequencies can be visible. As demonstrated in the plot, only the 60 and 180 Hz components are significantly above the noise and thus we can hope to manipulate the AC fields by just adjusting for these two peaks.

7.1.2 Finesse of the coils

Tuning Parameters

One aspect of ensuring that the apparatus is functional is that we are able to tune the system in a manner that allows us to find the optimal settings for canceling the fields. There are a few different parameters that can be tuned, as listed:

- The potentiometer that controls the balance between the two inputs in the summer
- The potentiometer controlling the input gain
- The potentiometer controlling the output gain
- Digital code controlling the delay of the entire signal
- Digital code controlling the overall gain
- Digital code controlling the magnitude and phase of the DC, 60 Hz, and 180 Hz components of the signal.

We found that the input analog controls were suitable for ensuring that the values were within range of the inputs of the ADC, but that manipulation of the wave function was most suitably done through the digital control, with the magnitude and phase factor controlling the frequency components.

We wanted to ensure that when manipulating the transfer function, we could target only the harmonics of the 60 Hz frequency, so we tested the apparatus by providing a 60 Hz and 180 Hz signal at a sampling frequency of 14.2 KHz and measuring the transfer function, as seen in figure 7-1. We see that for both plots, besides the DC component, only a single peak is significantly above the noise, corresponding to 60 and 180 Hz. Thus we can trust the peaks spectrum as shown in figure 7-2 to be accurate in measuring only the 60 and 180 Hz components respectively and thus can manipulate them in the output without significant mixing.

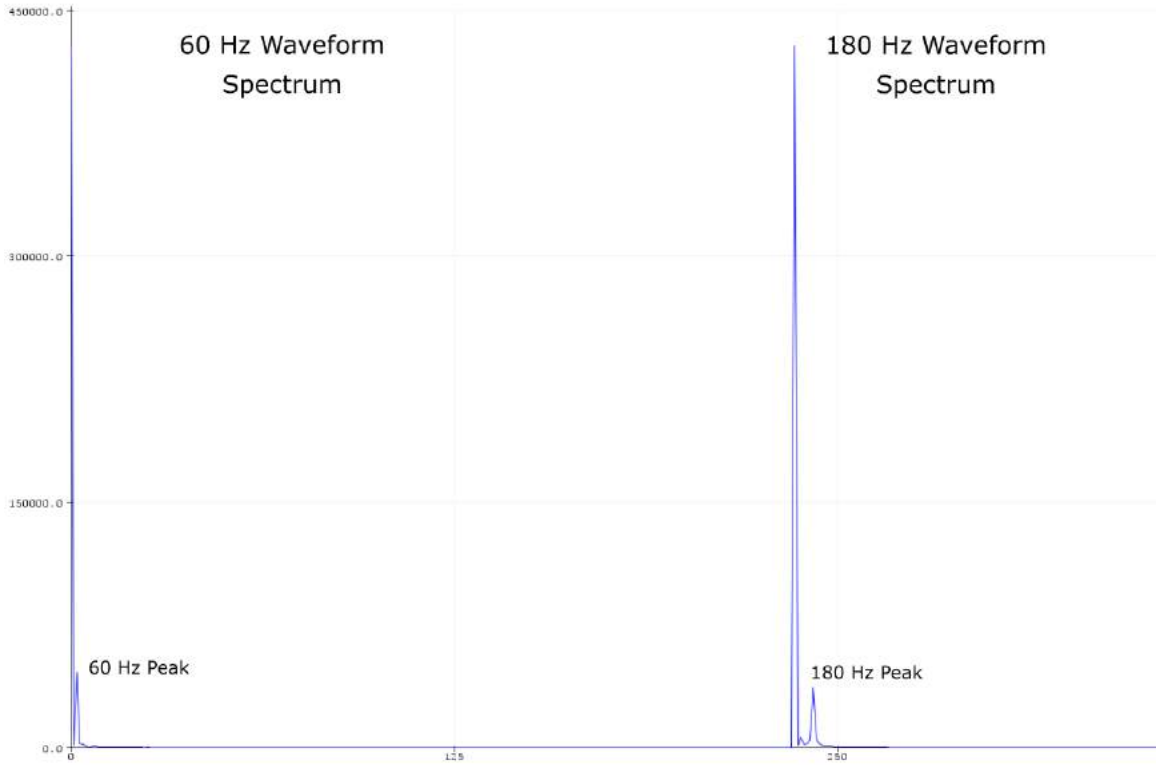

Figure 7-1: Plot of Amplitude vs Frequency. The current driver is running a 60 Hz and 180 Hz signal from a function generator, which is making the single visible peak. The left set of peaks come from running the 60 Hz signal and the right set of peaks comes from running the 180 Hz signal.

7.1.3 Improvement in AC and DC cancellation

A good question to ask is how easy is it to achieve the results desired. Optimally, we would like to simply be able to connect the apparatus, turn on the coils, and see immediate results. The results are actually a bit more complicated than that. Due to the non-trivial transfer function of the coils, we needed to adjust the gain and phase of each component.

We measured multiple runs of the apparatus, tuning the magnitude and phase of the DC, 60 Hz, and 180 Hz components within the code to achieve optimal status. I found that, for the specific current driver used, I achieved the optimal conditions with the settings listed in table 7.1, giving a reduction of 30±2 dB in the 60 Hz component and 20±2 dB in the 180 Hz component. The initial waveform had an average of 857 mV or 8.5 mT and RMS of 26.4 mV or 264 nT. The final setup had an RMS of 3.7

Component	Magnitude	Phase (Rad)
DC	1	
60 Hz	3.0	-0.95
180 Hz	7.0	-1.15

Table 7.1: Settings for optimal performance in setup used.

mV or 37 nT and DC of 287 mV or 2.87 mT. The DC component could be reduced further if properly tuned. Another, earlier run is shown in the comparison between figure 7-3 and figure 7-4, showing a drop of 20±2 dB in the 60 Hz component and 12±2 dB in the 180 Hz component. This setting would remain optimal for multiple minutes. These settings are sensitive to the location and orientation of the Helmholtz coil and the current driver proportional and derivative gain parameters.

In regards to the sensitivity of the parameters, I found that the most significant issue came from how sensitive the performance is to the phase angle. If the angle of either the 60 or 180 Hz phase parameter was off from the optimal value by 0.5 rads, the 60 Hz changes from -30 dB to -20 dB, after which the drop was less significant with change in phase, which means at least 0.5 rad precision was needed to optimize the setup.

When measuring the DC component, we found that it depended on the surrounding equipment, as any electrical equipment and surrounding metal, including the shelves, quickly changed the transfer function. In addition, DC cancellation was only effective when the setup was orientated vertically to minimize dependence of the B-field on the angle of orientation. It would be optimal to be able to cancel all 3 axis simultaneously to reduce dependency on orientation.

7.2 Tuning Method

To optimally tune the setup in the current state, I would use the function generators to send in 60 Hz, 180 Hz, and 1 Hz wave forms to approximate the open loop transfer function at the input to the current driver, and then fine tune these approximations by adjusting the phase and gain of the DC, 60 Hz, and 180 Hz Fourier components

until the optimal settings were achieved, using the oscilloscope to monitor the noise in the middle of the coils.

This is impractical for the actual consideration, so a more practical method is to use Feshbach spectroscopy to tune the AC fields. First setup the system such that the DC field is minimized, which can be done by knowing the gain of the apparatus and measuring the average of the magnetometers beforehand. Then find a Feshbach resonance to use as a proxy for the B-field. Once a resonance peak is detected, pick the current such that the field is to the side of the peak, where the value is most sensitive to fluctuations in the magnetic field. There we expect significant loss due to the AC noise. Then by adjusting the gain and phase of the AC components, one can expect to increase the efficiency of producing Feshbach molecules, thus serving as a proxy for how well are our tuning of the phase and magnitude. Optimize the parameters and we should have an optimal setup for canceling the fields.

7.3 Conclusion

I found that it is possible to minimize the magnetic field to an acceptable level of 37 nT. Some noise still existed which prevents us from reaching the target level of 4.3 nT that was achieved in [16]. Limitations most likely exists due to ground loops that were unaccounted for as well as additional high frequency noise being picked out, which became especially prominent after adding the ADC and DAC. Cancellation of the DC component was only 66% but can be easily improved digitally with more careful tuning.

The status of the current experiment and out of control influences prevented additional measurements and the actual implementation of this apparatus into the current molecule forming experimental setup. It is my hope that this report would be of use to anyone who is interested in applying my setup to improve the efficiency of ongoing experiments.

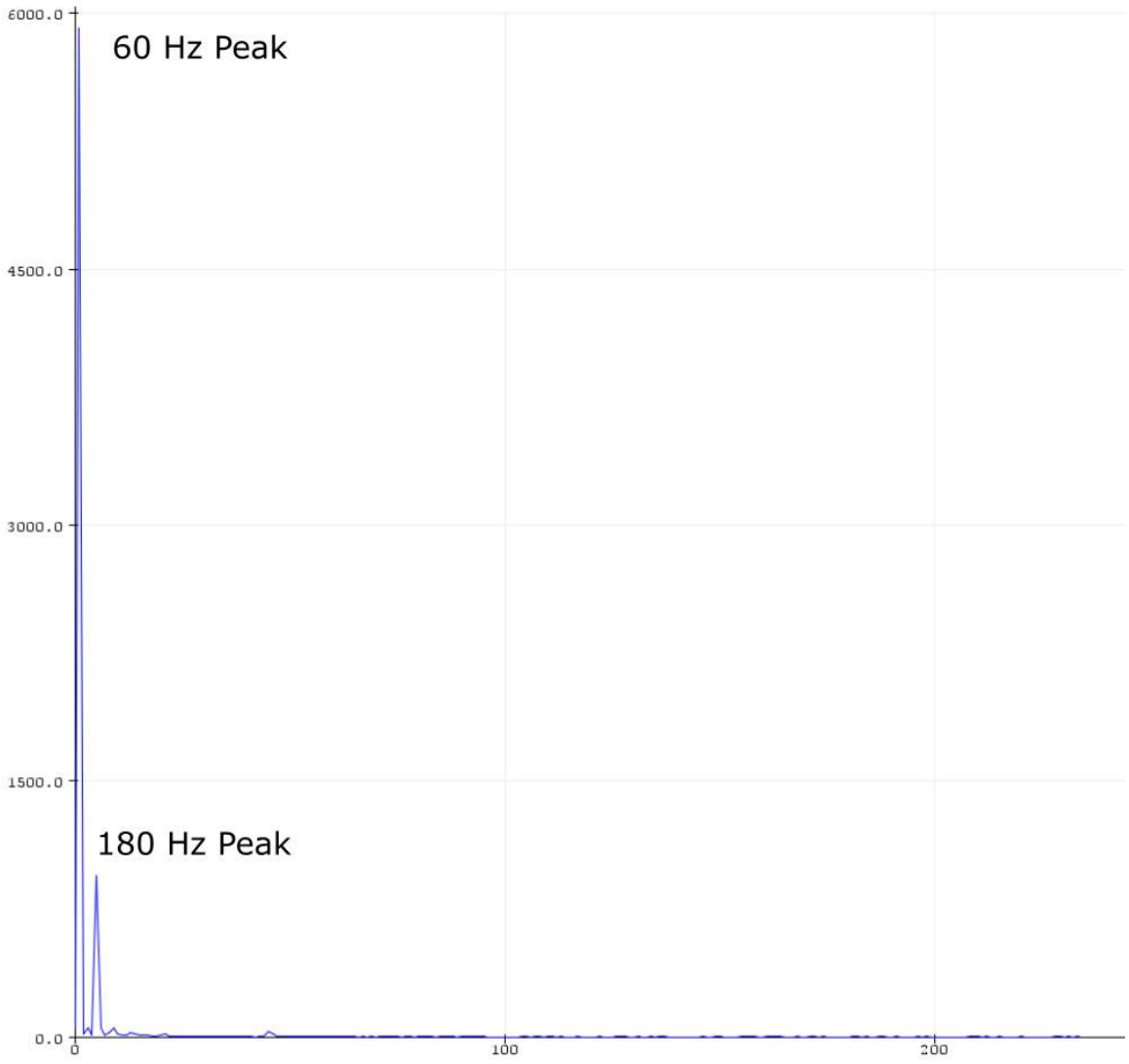

Figure 7-2: Plot of Amplitude vs Frequency. The current driver is off, so the signal above is the actual noise spectrum detected by the setup. It is clear that the 60 Hz and 180 Hz are dominant and identifiable and can be individually manipulated to change the output signal. The DC component has been cut off to clearly see the peaks in the ambient noise.

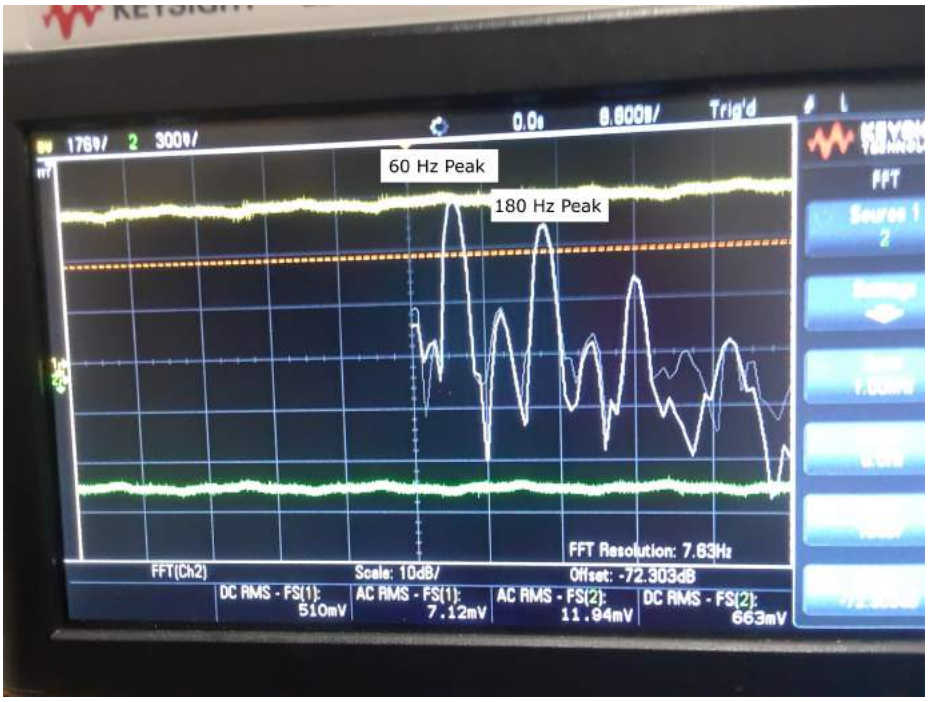

Figure 7-3: Image of the Oscilloscope reading of the Magnetic Field in the setup with the corresponding FFT spectrum before cancellation. The field was originally an average of 6.6 μT and RMS of 120 nT.

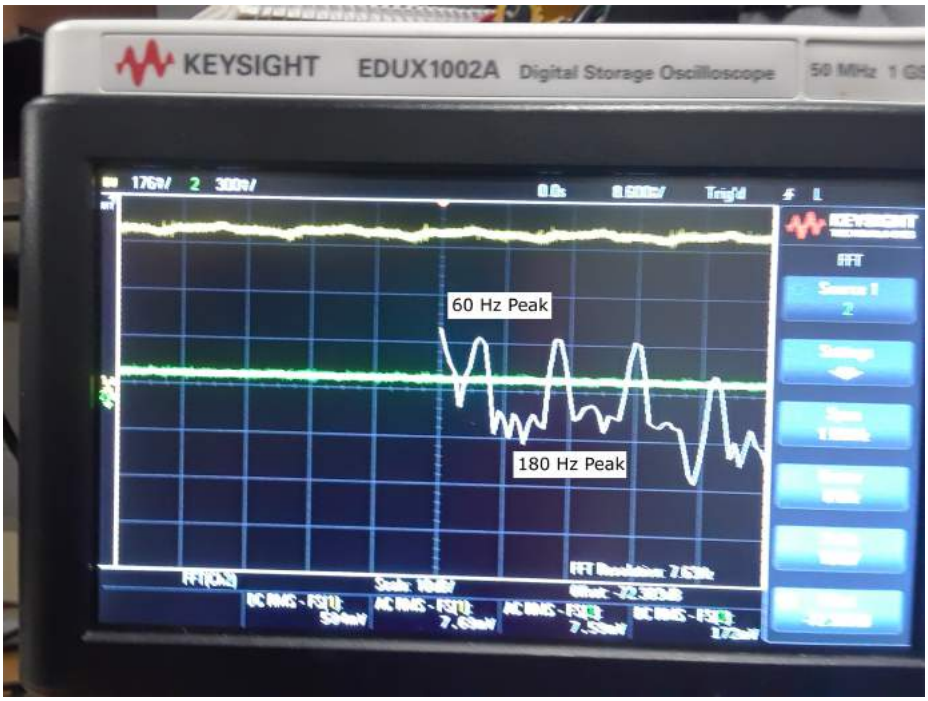

Figure 7-4: Image of the Oscilloscope reading of the Magnetic Field in the setup with the corresponding FFT spectrum after cancellation. We detect a 20 dB drop in the spectrum for 60 Hz and a 15 dB drop in the spectrum for 180 Hz compared to figure 7-3. This gives an average field of 1.73 μT and RMS of 76 nT.

Bibliography

[1] K. B. Davis, M. O. Mewes, M. R. Andrews, N. J. van Druten, D. S. Durfee, D. M. Kurn, and W. Ketterle. Bose-einstein condensation in a gas of sodium atoms. *Phys. Rev. Lett.*, 75:3969–3973, Nov 1995.

[2] M. H. Anderson, J. R. Ensher, M. R. Matthews, C. E. Wieman, and E. A. Cornell. Observation of bose-einstein condensation in a dilute atomic vapor. *Science*, 269(5221):198–201, 1995.

[3] W Ketterle. Bose–einstein condensation in dilute atomic gases: atomic physics meets condensed matter physics. *Physica B: Condensed Matter*, 280(1):11 – 19, 2000.

[4] Timur M. Rvachov, Hyungmok Son, Ariel T. Sommer, Sepehr Ebadi, Juliana J. Park, Martin W. Zwierlein, Wolfgang Ketterle, and Alan O. Jamison. Long-lived ultracold molecules with electric and magnetic dipole moments. *Phys. Rev. Lett.*, 119:143001, Oct 2017.

[5] Caleb A Christansen. *Ultracold Molecules from Ultracold Atoms: Interactions in Sodium and Lithium Gas*. PhD dissertation, Massachusetts Institute of Technology, Department of Physics, 2011.

[6] Xiao-Gang Wen. Statistical physics ii lecture, March 2019.

[7] C.J. Foot. *Atomic physics*. Oxford master series in physics. Oxford University Press, 2005.

[8] Wolfgang Ketterle and N.J. Van Druten. Evaporative cooling of trapped atoms. volume 37 of *Advances In Atomic, Molecular, and Optical Physics*, pages 181 – 236. Academic Press, 1996.

[9] Cheng Chin, Rudolf Grimm, Paul Julienne, and Eite Tiesinga. Feshbach resonances in ultracold gases. *Rev. Mod. Phys.*, 82:1225–1286, Apr 2010.

[10] Kristian Baumann, Nathaniel Q. Burdick, Mingwu Lu, and Benjamin L. Lev. Observation of low-field fano-feshbach resonances in ultracold gases of dysprosium. *Phys. Rev. A*, 89:020701, Feb 2014.

[11] Bela Bauer, Sergey Bravyi, Mario Motta, and Garnet Kin-Lic Chan. Quantum algorithms for quantum chemistry and quantum materials science, 2020.

[12] Alexander Prehn, Martin Ibrügger, Rosa Glöckner, Gerhard Rempe, and Martin Zeppenfeld. Optoelectrical cooling of polar molecules to submillikelvin temperatures. *Phys. Rev. Lett.*, 116:063005, Feb 2016.

[13] Hsin-I Lu, Ivan Kozyryev, Boerge Hemmerling, Julia Piskorski, and John M. Doyle. Magnetic trapping of molecules via optical loading and magnetic slowing. *Phys. Rev. Lett.*, 112:113006, Mar 2014.

[14] Lawrence W. Cheuk, Loïc Anderegg, Benjamin L. Augenbraun, Yicheng Bao, Sean Burchesky, Wolfgang Ketterle, and John M. Doyle. Λ-enhanced imaging of molecules in an optical trap. *Phys. Rev. Lett.*, 121:083201, Aug 2018.

[15] Nikolay V. Vitanov, Andon A. Rangelov, Bruce W. Shore, and Klaas Bergmann. Stimulated raman adiabatic passage in physics, chemistry, and beyond. *Rev. Mod. Phys.*, 89:015006, Mar 2017.

[16] B. Merkel, K. Thirumalai, J. E. Tarlton, V. M. Schäfer, C. J. Ballance, T. P. Harty, and D. M. Lucas. Magnetic field stabilization system for atomic physics experiments. *Review of Scientific Instruments*, 90(4):044702, Apr 2019.

[17] Texas Instruments. *ADS131A0x 2- or 4-Channel, 24-Bit, 128-kSPS, Simultaneous-Sampling, Delta-Sigma ADC*, 3 2016. Rev. January 2018.

[18] Linear Technology. *Quad 16-Bit/12-Bit 10V VOUT SoftSpan DACs with 10ppm/C Max Reference*, 6 2016. Rev. A.

Appendix A

Guide to using SPI on an Arduino

Often times we wish to send instructions and digital data between devices in a fast and reliable manner. The fastest method would be to send the data in multiple channels for each bit simultaneously and use various logic gates to process them, but when working with large data values, going up to 12 and 16 bits, the number of required channels increases significantly, which quickly becomes unwieldy. Thus, serial communication is often preferred, which sends the bits sequentially to transmit information.

Most interfaces nowadays uses serial communication, and a variety of protocols exist to transmit data for storage and communication. This includes USB, Ethernet, I2C, PCI Express, and many more, with different advantages and uses in terms of amount of and speed of information transmitted.

To optimize speed while minimizing channel ports, SPI was chosen because it had a minimum requirement of 4 channels, 2 for simultaneous communication, and could be connected easily to multiple devices with a minimal number of pins. In addition, Arduinos contained libraries for interfacing through SPI. Here we will describe how SPI functions and how to set up an Arduino to utilize SPI communication.

A.1 Explanation of SPI

SPI, or Serial Protocol Interface, is a commonly used protocol used for fast speed communication. It utilizes 4 channels: a Select Channel, two one-way channels, and a clock channel, as shown in figure A-1.

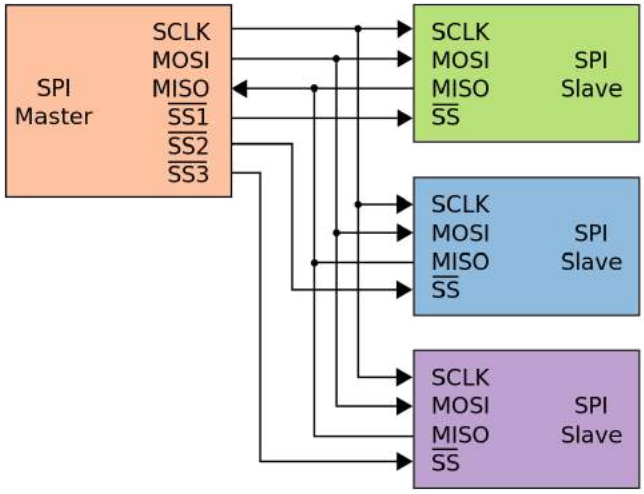

Figure A-1: Multiple SPI slave devices are connected with a master device. The slave devices can share the SCLK, MOSI, and MISO channels, but require independent SS channels.

One device, in our case the Arduino, is chosen as the master and all other channels are chosen as the slaves. To synchronize all devices, we send the clock channel (SCLK) from the Arduino to the others, making sure that the clock-speed of the Arduino is slower than the slave's maximum speed. The clock is used to determine sequentially what input bits are being fed in.

The select channel (SS) is utilized to signal to the device when to start reading a sequence of bits, or word, to determine the instruction or value desired. The pin is usually kept at a high voltage V_{dd} until SPI is ready to start. It is then brought to 0 voltage, at which the slave device recognizes that sequence has started. Once a given number of bits is inputted, which depends on the word length requirement for the device, the devices will ignore any additional bits until the select channel goes back to V_{dd}, at which point it will wait for the next word to appear.

We then have the 2 one-way channels. The MISO channel (Master In Slave Out) sends bits from the master device, in our case the Arduino, to the slave device. The MOSI channel (Master Out Slave In) sends bits from the slave device to be received by the master. Many devices have settings to determine whether it is a master or a slave, usually by providing a voltage to specific pins. When the select channel turns on, the MISO and MOSI channel each send a bit simultaneously according to the timing set by the clock channel. These channels continue transmitting until it has finished all the bits it wishes to send or select channel is turned off, at which point the MISO and MOSI channel are forced to 0V and can no longer transmit information.

One issue with SPI is that it is not an industry standard, but rather a common set of guidelines on how to perform serial communication. As such, there is no standard connection type, names for each channel may differ between devices, and there are differences between devices on how the timing for each bit in relation to the clock devices. There are usually four main timing schemes, or Modes, used, and the specific one can often be found in the manual for the devices. The four schemes can be seen in figure A-2. The parameters to watch for are the clock polarity and the clock phase.

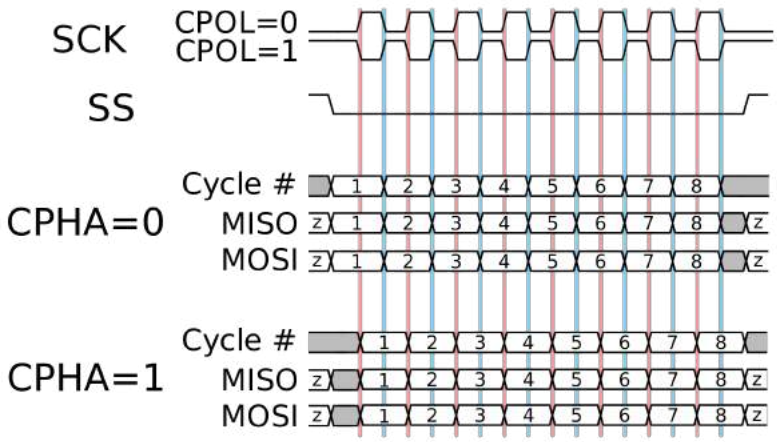

Figure A-2: The different timings and polarity settings for SPI are shown above. These different settings designate different Modes and should be checked for in the instruction manuals.

The clock polarity determines whether the clock is idle at 0 with CPOL=0, or 1 with CPOL=1. Each tick is registered when the voltage is flipped, which is called the

leading edge, and it returns to idle at the trailing edge. The clock phase tells you when the new bit is outputted, with CPHA=0 saying the new bit appears at the trailing edge, and CPHA=1 saying the new bit appears at the leading edge. The different modes and corresponding parameters are as follow:

Mode	CPOL	CPHA
SPI_MODE0	0	0
SPI_MODE1	0	1
SPI_MODE2	1	0
SPI_MODE3	1	1

To communicate with multiple devices through SPI, you can either connect all the devices to each other and signal which device to read with different select channels, which is more common and is seen in figure A-1, or you can daisy chain the channels.

A.2 Implementation of SPI on Arduino Due

We used the Arduino Due, which has a designated port for the SPI connections. The SPI pins are labeled in figure A-3. We chose other digital pins to act as our slave select channels.

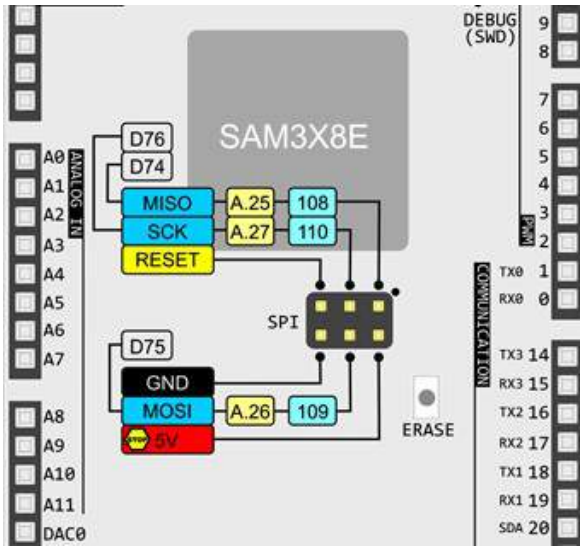

Figure A-3: The pinout for SPI on the Arduino Due is depicted above.

There are at least 2 libraries among the Arduino database that claim to use SPI, with varying successes. What follows are the instructions that worked best for us.

First include the SPI library. Then, in the setup command, you want to initialize SPI using "SPI.begins()". You then want to set the bit order as listed in the manual, either "MSBFIRST" or "LSBFIRST", which determines whether the first or last digit of the word is inputted and outputted first. You then need to set the clock divider, which determines the frequency of SCLK by dividing the internal clock frequency, which is 84 MHz for the Due. You also need to choose which mode to use. You can change the settings after each transmission if each slave device has different requirements. An example setup is shown in the following:

```
SPI.begin();
SPI.setBitOrder(MSBFIRST);
SPI.setClockDivider(8);
SPI.setDataMode(SPI_MODE1);
```

To transmit information, you need to determine how to read and write the code-words from the instruction manual for each device to transmit and receive data. All data are in binary numbers, and each byte of data are transmitted with the following:

```
a=SPI.transfer(0x00);
```

Note that you can send decimal and hexadecimal numbers and it will be translated to binary. The outputting value is stored in the given variable. You repeat this instruction until the code word is completed, at which point you will have the full output which can then be post processed. To send a word, you use a digital I/O channel as the select channel to choose the device with which to communicate by bringing it from high to low voltage, then send the desired numbers that make up the word.

A.3 SPI communication with ADS131A04EVM

To send instructions to the ADC, one sends a 8-bit message from the Arduino to the ADC. In the next message, an 8-bit output is also received that provides the status of the system, followed by a 16 bit message that provides the value of the voltage being read by the Arduino[17].

Before the ADC can be used, we must provide instructions to turn on the ADC, select settings, and read out the input value. These can be done by sending in register commands. We first unlock the ADC with the command "011001010101" or 0x655 in hexadecimal. "0x4E2F" writes to register E and changes the ADC modulator clock frequency to 1/2 of the internal clock frequency and changes the output frequency to 1/32 of the modulator clock frequency, while the command "0x4D02" writes to register D and changes the internal clock frequency to 1/2 of the signal clock frequency, maximizing the data output rate. "0x4F0F" writes to register F and enables all ADC channels and "0x0033" calls for the ADC to wakeup and start outputting the voltage readouts.

To read the voltage out of the range -2.5V to 2.5V, one sends in 24 bits of 0, for which from the message received, the first 8 bits gives a status readout and the next 16 bits provides the corresponding voltage value.

A.4 SPI communication with LTC2664

Communication with the DAC is simpler. We send a code word that tells the DAC to output the voltage at a selected channel by sending out "0011" to instruct the DAC to save and push out the provided and "0001" to select the first output channel. We then send out the value of the voltage as a 16 bit binary number that divides evenly the selected range [18].